



This is a repository copy of *Structural size optimization of single and built-up cold-formed steel beam-column members*.

White Rose Research Online URL for this paper:
<https://eprints.whiterose.ac.uk/181964/>

Version: Accepted Version

Article:

Mojtabaei, S.M. orcid.org/0000-0002-4876-4857, Becque, J. and Hajirasouliha, I. orcid.org/0000-0003-2597-8200 (2021) Structural size optimization of single and built-up cold-formed steel beam-column members. *Journal of Structural Engineering*, 147 (4). 04021030. ISSN 0733-9445

[https://doi.org/10.1061/\(asce\)st.1943-541x.0002987](https://doi.org/10.1061/(asce)st.1943-541x.0002987)

This material may be downloaded for personal use only. Any other use requires prior permission of the American Society of Civil Engineers. This material may be found at [https://doi.org/10.1061/\(ASCE\)ST.1943-541X.0002987](https://doi.org/10.1061/(ASCE)ST.1943-541X.0002987).

Reuse

Items deposited in White Rose Research Online are protected by copyright, with all rights reserved unless indicated otherwise. They may be downloaded and/or printed for private study, or other acts as permitted by national copyright laws. The publisher or other rights holders may allow further reproduction and re-use of the full text version. This is indicated by the licence information on the White Rose Research Online record for the item.

Takedown

If you consider content in White Rose Research Online to be in breach of UK law, please notify us by emailing eprints@whiterose.ac.uk including the URL of the record and the reason for the withdrawal request.



eprints@whiterose.ac.uk
<https://eprints.whiterose.ac.uk/>

Structural Size Optimisation of Single and Built-Up Cold-Formed Steel Beam-Column Members

Seyed Mohammad Mojtabaei¹, Jurgen Becque², and Iman Hajirasouliha³

¹EPSRC Research Fellow, Dept. of Civil and Structural Engineering, Univ. of Sheffield, Sheffield S1 3JD, UK (corresponding author). ORCID: <https://orcid.org/0000-0002-4876-4857>. Email: smmojtabaei@sheffield.ac.uk

²Lecturer, Dept. of Engineering, Univ. of Cambridge, Cambridge CB2 1PZ, UK. Email: jurgen.becque@eng.cam.ac.uk

³Senior Lecturer, Dept. of Civil and Structural Engineering, Univ. of Sheffield, Sheffield S1 3JD, UK. ORCID: <https://orcid.org/0000-0003-2597-8200>. Email: i.hajirasouliha@sheffield.ac.uk

Abstract

The use of cold-formed steel elements in residential and industrial buildings is widely gaining popularity due to their ability to provide cost-effective and sustainable solutions. A high degree of flexibility in the manufacturing of various cross-sectional shapes provides a unique opportunity to further improve the load-carrying capacity of these elements through an optimisation process, leading to more efficient and economical structural systems. This paper aims to offer a practical methodology for the optimum design of CFS beam-column members with different lengths and thicknesses, subject to various combinations of axial compression and bending moment, but with constant material use. The optimisation process is carried out using a Genetic Algorithm and aims to maximise the resistances of CFS members, determined according to the Eurocode 3 design guidelines. Six initial prototype cross-sections, including both single and built-up channel sections, are selected and their relative dimensions and edge stiffener configurations are allowed to vary during the optimisation process. To ensure practically relevant solutions EC3 slenderness constraints, as well as a range of practical manufacturing and construction limitations, are imposed on the cross-sections. Standard commercially available single and back-to-back lipped channel sections are taken as the starting points of the optimisation and used to benchmark the efficiency of the optimised sections. Significant gains in capacity (of up to 156 % in the present study) can be obtained compared to the initial cross-sections, while the optimisation results also offer further insights on the material efficiency achievable with various cross-sectional shapes in combined loading scenarios ranging from pure bending to pure compression.

Keywords

cold-formed steel (CFS); optimisation; beam-column; buckling; material efficiency

1 Introduction

Cold-formed steel (CFS) structural members are fabricated at room temperature from thin gauge steel sheets. They offer several advantages over conventional hot-rolled steel products, such as a higher strength-to-weight ratio, a highly flexible manufacturing process and a light weight, leading to easier handling, transportation and installation. CFS products have traditionally been used as secondary structural members, such as purlins, girts (side rails), stud walls and mezzanine floors. However, over the past few decades their market share has expanded into applications where they are used as the primary load-bearing structure, most notably in multi-storey CFS buildings and CFS portal frames for commercial and industrial buildings (Mojtabaei et al., 2018). In many of those practical applications, CFS members are subjected to a combination of axial compression and bending, and this has prompted several research studies into CFS members under combined actions (Cheng et al., 2013, Ma et al., 2019, Li and Young, 2019). Combined loading may originate from eccentrically applied loads, as shown in Fig. 1(a), where the eccentricity is in some cases caused by the shift of the effective centroid of the cross-section due to local or distortional buckling. Furthermore, in CFS portal frames all members are subject to combined axial compression and bending moments due to the rigidity of the connections (Fig. 1 (b)). A third example is provided in Fig. 1(c) and relates, for instance, to stud walls around the perimeter of a building, which resist both gravity loading and wind loads. Combined actions may also originate in an analysis accounting for nominal imperfections in the structure according to the Eurocodes (CEN, 2005a, CEN, 2005b, CEN, 2006).

Previous studies have investigated the behavior of CFS beam-column members under various load combinations and compared the results with the available design codes. Torabian et al. (2015, 2016) experimentally investigated the buckling resistance of CFS beam-columns with lipped channel and Z cross-sections under bi-axial moments and axial force. The results were subsequently used to assess the

reliability of the North American design standard (AISI S100-12) and to propose improvements to the linear interaction equation, which was proven to be conservative.

Cheng et al. (2013) studied channel sections subject to combined compression and minor and major axis bending by analytical means, using a variational principle. Ma et al. (2019) tested 51 cold-formed high-strength steel square and rectangular hollow section beam-columns. For the rectangular sections both the cases of minor and major axis bending in combination with compression were considered. The experimental results were compared to the predictions of the North American (ANSI/AISC 360-10), European EN1993-1-1 (CEN, 2005b) and Australian design provisions (AS 4100:1990 Steel Structures), which were generally found to be slightly conservative. The work by Li and Young (2019) also deserves mention. The authors conducted 15 eccentric compression tests on built-up specimens, consisting of two identical channels with both intermediate and edge stiffeners connected back-to-back using self-tapping screws. The North American AISI standards (AISI S100-12) were found to be conservative for this type of cross-section.

A significant amount of previous research has focused on improving the behaviour of CFS elements under single actions (i.e. either bending or axial compression) in terms of their strength, stiffness and energy dissipation by optimising the cross-sectional shape. These optimisation studies can be divided into two categories: (i) optimisation without any restrictions on the overall shape of the cross-section (i.e. unconstrained shape optimisation) (Liu et al., 2004, Leng et al., 2011, Gilbert et al., 2012a, Gilbert et al., 2012b, Sharafi et al., 2014, Madeira et al., 2015, Wang et al., 2016a), and (ii) optimisation of the relative dimensions of a predefined cross-sectional shape (i.e. size optimisation) (Adeli and Karim, 1997, Karim and Adeli, 1999, Tian and Lu, 2004, Lee et al., 2005, Magnucki et al., 2006, Tran and Li, 2006, Pastor et al., 2009, Leng et al., 2014, Ma et al., 2015, Ye et al., 2016a, Wang et al., 2016b, Wang et al., 2016c, Ye et al., 2018b, Ye et al., 2018a, Ye et al., 2018c, Mojtabaei et al., 2019, Lee et al., 2006, Phan et al., 2019). The latter tend to result in more practical and manufacturable solutions, but do not yield absolute overall optima. Various optimisation algorithms have been employed in the past to

optimise CFS elements, such as Graph Theory and Ant Colony Optimisation (Sharafi et al., 2014), Genetic Algorithms (GA) (Wang et al., 2016a, Gilbert et al., 2012b, Lee et al., 2005, Ma et al., 2015), Particle Swarm Optimisation (PSO) (Ye et al., 2016a, Ye et al., 2018b, Ye et al., 2016b), Direct Multi-Search optimisation (DMS) (Madeira et al., 2015), the Big Bang-Big Crunch algorithm (BB-BC) (Mojtabaei et al., 2019), simulated annealing and the gradient-based steepest descent method (Leng et al., 2011). Ye et al. (2016a) previously showed that the flexural capacity of a standard commercially available CFS channel could be noticeably enhanced by performing a size optimisation and adjusting the cross-sectional dimensions. To further improve the beam capacity, the investigators optimised a wide range of cross-sectional shapes comprising edge and intermediate stiffeners, as well as segmentally folded flanges (Ye et al., 2016b). Mojtabaei et al. (2019) also optimised CFS beams, but considered both ultimate and serviceability limit state conditions. In another relevant study by Ye et al. (2018a) CFS beam sections were optimised for maximum energy dissipation to improve their seismic characteristics.

A significant amount of optimisation work has also been carried out on CFS columns. An unconstrained shape optimisation study (Leng et al., 2014) showed that the compressive capacity of CFS elements can be significantly increased (by up to 140%) compared to the available standard cross-sectional shapes. In another relevant study, Ma et al. (2015) optimised channel shapes, while allowing intermediate stiffeners, inclined lips and return lips to appear in the cross-section. Genetic Algorithms were used and a range of practical constraints was considered in the optimisation process. Along similar lines Lee et al. (2006) conducted a constrained shape optimisation to improve the compressive strength of CFS members and presented optimum design curves for various levels of loading.

In terms of optimisation at the frame level, most of the previous studies have been conducted for portal frames composed of hot-rolled steel sections (e.g. (McKinstry et al., 2015, McKinstry et al., 2016)). As a rare exception, Phan et al. (2019) developed a coupled element and structural level

optimisation framework to improve the structural performance of CFS portal frames at the serviceability and ultimate limit states.

In contrast to the relatively large body of work pertaining to CFS members in pure bending or pure compression, only a very limited number of previous studies have investigated the optimum design of CFS beam-column elements subject to various combinations of bending and compression. Wang et al. (2016a) conducted the first shape optimisation study of simply supported CFS beam-columns using the Direct Strength Method (DSM). In a more recent study, a similar approach was adopted by Parastesh et al. (2019) to carry out shape optimisation of CFS beam-columns with singly-symmetric open cross-sections using GA. However, their optimised cross-sections consisted of complex curved shapes, which may not be suitable for practical applications.

This paper presents a practical methodology for the optimum design of CFS beam-column members with different lengths and thicknesses, subject to various combinations of axial compression and bending moment, while keeping the material use constant. The optimisation process was carried out with respect to the member resistances determined according to Eurocode 3 (EC3) (CEN, 2005a, CEN, 2005b, CEN, 2006) using a GA. It is noted that the design of beam-columns to EC3 can be a tedious task, since the capacity of the element is simultaneously controlled by different types of instabilities (i.e. local, distortional and global buckling modes). Six different cross-section prototypes, including both single and built-up channel sections, were considered. They were individually optimised using a size optimisation process, with their relative dimensions and the inclination of the lip stiffeners considered to be the main design variables. To ensure practical results which are relevant to industry, the EC3 plate slenderness limits, as well as a number of practical manufacturing and construction constraints, were imposed. The resistances of the optimized beam-columns were compared to those of standard commercially available sections with the same weight. The observed evolution in the cross-sectional shape over the spectrum ranging from pure compression to pure bending is also discussed.

2 Eurocode design procedure for beam-column members

In this study the capacity of CFS beam-column elements was determined according to EN1993-1-1 (CEN, 2005b), EN1993-1-3 (CEN, 2005a) and EN1993-1-5 (CEN, 2006), following two main steps: (i) a check on the cross-section resistance, accounting for both local and distortional buckling modes, and (ii) a check on the member resistance, considering global instabilities. Employing Clause 5.1 of EN1993-1-3, the cross-sectional properties were first calculated based on the equivalent cross-section with sharp corners and subsequently corrected for the presence of rounded corners using the prescribed reduction factors.

2.1 Cross-section resistance

2.1.1 Local buckling

EC3 accounts for local buckling through the effective width method, which is based on the fact that local buckling leads to a loss of load-bearing capacity in the center of a plate supported along both longitudinal edges, or along the free edge of a plate supported along one longitudinal edge. Longitudinal strips adjacent to the corner zones consequently become the main load-resisting parts of the cross-section. In general, local buckling causes the centroid of the effective cross-section to shift over a distance e_N relative to the original centroid of the gross cross-section, which may cause additional bending moments in a cross-section subject to compression. For cross-sections subject to bending an iterative process is required to find the neutral axis of the effective cross-section. Fig. 2 illustrates the effective areas of a lipped channel (in solid black line) under axial compression (Fig. 2a), bending about the major axis (Fig. 2b) and bending about the minor axis with the web in either compression or tension (Figs. 2c and 2d).

In the case of minor axis bending causing compression in the web (Fig. 2c), yielding initiates in the lips located on the tension side, while the compression part is still in the elastic range. In this case EN 1993-1-3 (CEN, 2005a) allows the inelastic reserve capacity in the tension zone to be utilized without strain limit until the most compressed fibre reaches the yield stress ($\sigma_c = f_y$). The bending capacity may

then be calculated using the effective partially plastic section modulus $W_{pl,eff}$ based on the bilinear stress distribution shown in Fig. 3.

2.1.2 Distortional buckling

Distortional buckling can be interpreted as flexural or flexural–torsional buckling of an assembly consisting of a stiffener and its adjacent plate(s), and is characterized by both out-of-plane and in-plane displacements of some of the fold lines of the section. Distortional buckling can be associated with an edge stiffener, as seen in the flexural-torsional movement of the flange-lip subassembly of a lipped channel, or with an intermediate stiffener, as seen for instance in stiffened webs. In EC3 the effects of distortional buckling are taken into account by reducing the effective thickness of the stiffener and the adjacent (effective) parts of the stiffened plate. The calculations are based on a rational model where the stiffened subassembly of the cross-section acts as a compression element continuously supported by elastic springs with a stiffness K per unit length, as shown in Fig. 4. The elastic buckling stress $\sigma_{cr,s}$ of this column on an elastic foundation (and thus the distortional buckling stress) is calculated as:

$$\sigma_{cr,s} = \frac{2\sqrt{KEI_s}}{A_s} \quad (1)$$

where E is the Young's modulus, I_s is the second moment of area of the stiffener assembly about an axis through its centroid parallel to the stiffened plate and A_s is the cross-sectional area of the stiffener assembly. A distortional slenderness can then be defined based on the yield stress of the material f_y and the elastic buckling stress $\sigma_{cr,s}$:

$$\lambda_d = \sqrt{\frac{f_y}{\sigma_{cr,s}}} \quad (2)$$

For a given λ_d EC3 provides direct equations to calculate a reduction factor χ_d , which is applied to the thickness of the stiffener assembly.

2.1.3 Cross-section check

Each cross-section of a CFS beam-column subject to combined axial compression (N_{Ed}) and bending moments ($M_{y,Ed}$ and $M_{z,Ed}$) should satisfy the following requirement:

$$\frac{N_{Ed}}{N_{c,Rd}} + \frac{M_{y,Ed} + \Delta M_{y,Ed}}{M_{cy,Rd}} + \frac{M_{z,Ed} + \Delta M_{z,Ed}}{M_{cz,Rd}} \leq 1 \quad (3)$$

In the above equation $N_{c,Rd}$ is the design compressive resistance of the cross-section, while $M_{cy,Rd}$ and $M_{cz,Rd}$ are the design moment resistances about the major (y) and the minor (z) axes, respectively. The additional moments $\Delta M_{y,Ed}$ and $\Delta M_{z,Ed}$ are generated by the shifts of the centroidal axes of the effective cross-section relative to those of the gross cross-section, and are given by:

$$\Delta M_{y,Ed} = N_{Ed} e_{Ny} \quad (4)$$

$$\Delta M_{z,Ed} = N_{Ed} e_{Nz} \quad (5)$$

where e_{Ny} and e_{Nz} are the shifts of the y- and z-axis, respectively.

2.2 Member resistance

The verification of the member stability of a beam-column requires the separate calculation of the member resistances in pure compression and pure bending.

2.2.1 Global buckling of a member subjected to pure compression

The design buckling resistance of a compression member ($N_{b,Rd}$) for flexural buckling about the y- and z- axes, torsional or flexural-torsional buckling is determined by:

$$N_{b,Rd} = \frac{\chi A_{eff} f_y}{\gamma_{M1}} \quad (6)$$

where A_{eff} is the effective cross-sectional area, γ_{M1} (= 1.0) is the partial safety factor and χ is a reduction factor based on the column slenderness $\bar{\lambda}$:

$$\chi = \frac{1}{\phi + \sqrt{\phi^2 - \bar{\lambda}^2}}, \quad \left\{ \begin{array}{l} \phi = 0.5[1 + \alpha(\bar{\lambda} - 0.2) + \bar{\lambda}^2] \\ \bar{\lambda} = \sqrt{\frac{A_{eff} f_y}{N_{cr}}} \end{array} \right\} \quad (7)$$

In the above equation, α accounts for the effect of imperfections through the adoption of an appropriate buckling curve and N_{cr} is the elastic critical buckling load for the relevant buckling mode:

- For flexural buckling about the y-axis:
$$N_{cr,Fy} = \frac{\pi^2 EI_y}{L_{cr}^2} \quad (8)$$

- For flexural buckling about the z-axis:
$$N_{cr,Fz} = \frac{\pi^2 EI_z}{L_{cr}^2} \quad (9)$$

- For torsional buckling:
$$N_{cr,T} = \frac{1}{i_0^2} (GI_t + \frac{\pi^2 EI_w}{L_{cr}^2}) \quad (10)$$

- For flexural-torsional buckling:
$$N_{cr,FT} = \frac{N_{cr,Fy}}{2\beta} \left(1 + \frac{N_{cr,T}}{N_{cr,Fy}} - \sqrt{\left(1 + \frac{N_{cr,T}}{N_{cr,Fy}} \right)^2 - 4\beta \frac{N_{cr,T}}{N_{cr,Fy}}} \right) \quad (11)$$

In the above equations (8-11), I_y and I_z are the second moments of area of the gross cross-section about the y- and z-axes, respectively, I_t and I_w are the torsional and warping constants of the cross-section, respectively, L_{cr} is the buckling length for the relevant buckling mode and $i_0 = i_y^2 + i_z^2 + y_c^2 + z_c^2$ is the polar radius of gyration. i_y and i_z are the radius of gyration of the gross cross-section about the y- and z-axes, respectively, and y_c and z_c are the shear centre coordinates relative to the centroid. G is the shear modulus and β is equal to $1 - (\frac{y_c}{i_0})^2$. For $N_{Ed}/N_{cr} \leq 0.16$ and $\bar{\lambda} \leq 0.2$ the reduction factor $\chi = 1$.

2.2.2 Lateral-torsional buckling of a member subject to pure bending

In the case of laterally unbraced CFS elements subject to a major axis bending moment, EN 1993-1-1 (CEN, 2005b) specifies the design lateral-torsional buckling resistance ($M_{b,Rd}$) to be calculated as follows:

$$M_{b,Rd} = \chi_{LT} W_{eff,y} f_y / \gamma_{M1} \quad (12)$$

where $W_{eff,y}$ is the effective section modulus about the y-axis and χ_{LT} is the reduction factor for lateral-torsional buckling calculated using the following equation:

$$\chi_{LT} = \frac{1}{\phi_{LT} + \sqrt{\phi_{LT}^2 - \bar{\lambda}_{LT}^2}}, \quad \left\{ \begin{array}{l} \phi_{LT} = 0.5[1 + \alpha_{LT}(\bar{\lambda}_{LT} - 0.2) + \bar{\lambda}_{LT}^2] \\ \bar{\lambda}_{LT} = \sqrt{\frac{W_{eff,y} f_y}{M_{cr}}} \end{array} \right\} \quad (13)$$

In the above Eq. (13), $\bar{\lambda}_{LT}$ is the slenderness for lateral-torsional buckling, M_{cr} is the elastic critical buckling moment and α_{LT} is the imperfection factor, equal to 0.34 (buckling curve b) for CFS. Lateral-

torsional buckling may be disregarded ($\chi_{LT} = 1$) if $\bar{\lambda}_{LT} \leq 0.4$ and $M_{Ed,y}/M_{cr} \leq 0.16$. The elastic critical buckling moment of a simply-supported beam with free end warping, subject to a uniform bending moment, is given by (Simões da Silva et al., 2010):

$$M_{cr} = \frac{\pi}{L} \sqrt{EI_z(GI_t + \frac{\pi^2 EI_w}{L^2})} \quad (14)$$

where EI_z , GI_t and EI_w are the flexural rigidity about the minor axis, the torsional rigidity and the warping rigidity, respectively.

2.2.3 Member stability check

According to EN 1993-1-3, beam-column members which are subject to combined bending and axial compression should satisfy the following equations:

$$\frac{N_{Ed}}{\chi_{Fy} N_{Rk}/\gamma_{M1}} + k_{yy} \frac{M_{y,Ed} + \Delta M_{y,Ed}}{\chi_{LT} M_{y,Rk}/\gamma_{M1}} + k_{yz} \frac{M_{z,Ed} + \Delta M_{z,Ed}}{M_{z,Rk}/\gamma_{M1}} \leq 1 \quad (15)$$

$$\frac{N_{Ed}}{\chi_{Fz} N_{Rk}/\gamma_{M1}} + k_{zy} \frac{M_{y,Ed} + \Delta M_{y,Ed}}{\chi_{LT} M_{y,Rk}/\gamma_{M1}} + k_{zz} \frac{M_{z,Ed} + \Delta M_{z,Ed}}{M_{z,Rk}/\gamma_{M1}} \leq 1 \quad (16)$$

with

$$\begin{cases} N_{Rk} = f_y A_{eff} \\ M_{y,Rk} = f_y W_{eff,y} \\ M_{z,Rk} = f_y W_{eff,z} \end{cases} \quad (17)$$

In Eqs. (15) and (16), χ_{Fy} and χ_{Fz} are the reduction factors for flexural buckling about the y- and the z-axes, obtained from Eq. (7). These should be replaced by the reduction factor χ_{FT} for flexural-torsional buckling where relevant, e.g. when buckling about the major axis of a mono-symmetric channel is considered, as specified in (CEN, 2020). The interaction factors k_{yy} , k_{yz} , k_{zy} and k_{zz} were calculated using Annex A of EN1993-1-1 (CEN, 2005b).

3 Definition of the optimisation problem

The aim of the research presented in this paper consisted in optimizing CFS beam-column elements subjected to different combinations of an axial compressive load (N_{Ed}) and a major axis bending

moment ($M_{y,Ed}$). The bending moment was applied using an eccentric axial compressive load ($M_{y,Ed} = N_{Ed}e_y$), and therefore, the optimisation problem could be formulated as:

$$\max N_{Ed}(X) \quad (X_i^L \leq X_i \leq X_i^U; i = 1, \dots, n) \quad (18)$$

subject to the cross-section satisfying the cross-sectional and member checks (Eqs. 3, 15, 16).

In Eq. (18) X is a vector including all cross-sectional design variables X_i , which are restricted by a lower bound X_i^L and an upper bound X_i^U .

In this study a simply-supported beam-column element with ‘end-fork supports’ was considered, meaning that end rotations about both cross-sectional axes and warping were free to occur, but twisting about the longitudinal axis was prevented. Four different values of the eccentricity e_y were considered: $e_y = 0$ mm, 250 mm, 1000 mm and 10^5 mm. As shown in Fig. 5, six different cross-section prototypes were part of the study, including three single sections (a plain channel ①, a lipped channel ② and a lipped channel with a return lip ③), two built-up sections (back-to-back channels ④ and a diamond-shaped cross-section ⑤) and a rectangular hollow section (RHS) ⑥. A size optimisation with respect to the design variables X_i listed in Fig. 5 was performed for each cross-section, after which the overall optimum solution for a given eccentricity was determined as the one corresponding to the maximum capacity among the six prototypes. In practical terms, size optimisation of a prototype can be seen to correspond to configuring a ‘flexible line’, i.e. a rolling line where the rolls ordinarily remain in place (rather than being swapped for different ones when rolling different cross-sections), but their positions can be adjusted within certain limits to modify the dimensions of the product. It has the advantage that no extra tooling costs are required when changing the dimensions. However, the cross-section is limited to a certain shape (e.g. a lipped channel).

In regards to the built-up prototypes it should be noted that a simplified approach was used in two respects (mainly due to the lack of design guidance in EN1993-1-3 for built-up CFS members). First, it was assumed that the behaviour of the members was fully composite with respect to the overall

bending stiffness. Recent research (Phan, 2020) has shown that this situation can be achieved with good approximation by using at least one row of properly tightened bolts at the specimen ends. The same publication also provides guidance on how to calculate the torsion and warping constants of CFS built-up sections and these recommendations were followed in this paper. Second, with respect to cross-sectional instability, it was assumed that the components buckled individually, without restraining each other through contact or connections. Previous research on back-to-back channels (Ye et al., 2019) has indicated that this is a very reasonable assumption, since both channels will buckle in an anti-symmetric manner. A similar rationale can be put forward for the diamond-shaped cross-section. Fig. 5 also lists the appropriate buckling curve for each prototype cross-section for global buckling about the major (y) and minor axes (z) according to EN1993-1-3.

Two different plate thicknesses ($t = 1.5$ mm and $t = 3$ mm) and two different element lengths ($L = 3000$ mm and $L = 5000$ mm) were considered in the optimisation process. The total developed length of the cross-section (i.e. the coil width before rolling), and thus the material use and weight, were kept constant for a given thickness. This developed length was chosen to be $l = 453$ mm and $l = 906$ mm for the single and the built-up sections, respectively. The radius of the rounded corners (measured along the midline of the section) was taken as $2t$. The elastic modulus and the Poisson's ratio were 210 GPa and 0.3, respectively, while the yield stress was assumed to be $f_y = 350$ MPa. A commercially available channel cross-section with the same developed length of 453 mm was taken as a benchmark throughout the optimization process, both for the single and (in a back-to-back configuration) the built-up cross-sections, as pictured in Fig. 6. A comparison of the capacity of the optimized sections with that of the benchmark sections provided a measure of the effectiveness of the adopted optimisation procedure and the possible gains in capacity in practical applications. It should also be noted that, according to the cross-sectional classification system in EN 1993-1-1, all studied cross-sections were categorized as either Class 3 or Class 4 due to the high slenderness of their constituent plates.

In order to ensure that practically relevant cross-sections were obtained from the optimisation process, a number of construction and manufacturing constraints were imposed, as well as some design limits to ensure the cross-sections fell within the scope of EC3. These constraints are listed in Fig. 5 and can be summarized as follows:

- a) EC3 specifies flange slenderness limits of $b/t \leq 50$, $b/t \leq 60$ and $b/t \leq 90$ for channels ①, ② and ③, respectively.
- b) To meet the requirements of SCI Guide ED-017 (Way and Lawson, 2013) and make the connections of the CFS element to trapezoidal decking or plywood boards feasible, the minimum flange width of the channels (cross-sections ①, ②, ③ and ④) was restricted to 50 mm.
- c) Since the constituent channels of the diamond-shaped cross-section (section ⑤) are connected to each other through their flanges, the minimum width of these flanges was set to 25 mm to provide enough space for the fasteners.
- d) The minimum side dimension of the RHS section (⑥) was taken as 100 mm to ensure a reasonable aspect ratio.
- e) The edge stiffeners were required to fulfil the EC3 requirements regarding their slenderness (e.g. $c/t \leq 50$) and relative dimensions (e.g. $0.2 \leq c/b \leq 0.6$).
- f) Based on the recommendation of the industrial partner of this project, the minimum length of the edge stiffeners was taken as 10 mm (i.e. $c \geq 10$ mm and $d \geq 10$ mm). Smaller stiffeners cannot practically be rolled or brake-pressed.
- g) EC3 requires the angle θ of the edge stiffeners (see Fig. 5) to be between $\pi/4$ and $3\pi/4$.
- h) For the diamond-shaped section the inclination of the webs was restricted to $\pi/6 \leq \theta \leq \pi/3$ (see Fig. 5) in order to obtain a practically reasonable geometry.
- i) EC3 requires the web slenderness h/t to be less than 500.
- j) A geometric constraint was imposed onto cross-sections ②, ③, and ④ for the length c of the lips not to exceed half of the height of the web in order to avoid overlap.

4 Genetic Algorithm (GA) optimisation

Genetic Algorithm (GA) optimisation is a computational technique which mimics the Darwinian evolution theory based on “survival of the fittest” (Holland, 1962). While other search methods such as simulated annealing or taboo search use a single candidate solution which continually morphs during the search process to find the optimum configuration, GA instead evolves a whole population of potential solutions through special selection rules to optimise a fitness function (equivalent to the optimisation target) (Holland, 1962, Gerald et al., 1989, Andre et al., 2001). GA generates a random initial population of individuals, each characterized by their chromosomes. Each individual represents a candidate solution for the problem, while a chromosome corresponds to a key design parameter. In each generation the individuals are evaluated according to the fitness function and those with the lowest fitness are eliminated. The fittest individuals are allowed to reproduce and generate offspring, in which the chromosomes of the parents are combined through a cross-over operator. GAs have the advantage that they do not need any gradient information about the fitness function. They have previously demonstrated good performance in avoiding local optima and converging to a global optimum (Goldberg, 1989). A GA was selected in this research study because of the complex and highly non-linear nature of the problem. Compared to other optimisation algorithms previously employed by the authors (in particular PSO (Ye et al., 2016a) and BB-BC algorithms (Mojtabaei et al., 2019)) a similar ability to converge on the optimum solution was observed, albeit at a slighter faster convergence rate. However, since GAs (not unlike PSO and BB-BC) are stochastic in nature, it is recommended that the optimisation procedure is repeated in order to minimize the odds of obtaining a sub-optimal solution. In the present study, each optimisation was repeated five times. All design constraints were satisfied in every generation by restricting the allowable values of the design parameters to their respective ranges during the mutation and cross-over operations.

The optimisation required the development of two distinct pieces of software in MATLAB (Mathworks, 2011): one implementing the EC3 design rules as presented in Section 2, and one executing the GA optimisation. The GA population size was taken equal to 80 for all beam-column sections, while the number of GA generations was kept at 100. A sensitivity analysis with respect to the other GA parameters was also carried out. A first parameter, the *crossover probability*, controls how often crossover is performed in a generation. During crossover the offspring is generated by combining the chromosomes of the parents. In this study, this parameter was taken as $P_c = 0.9$. The *mutation probability* controls the possibility of a random mutation occurring in the chromosomes, thus promoting a more random search over a larger part of the search space. In the case of no mutation, the offspring is obtained after crossover without any change. This parameter was selected to be $P_m = 0.01$. To increase the probability of the GA finding the global optimum in the case of complex problems with several local optima, a niching technique was used to create and maintain several subpopulations within the search space (Shir, 2012). The *niching radius* (R_n) was taken as 0.25. In this study, it was observed that convergence on the optimum solution was typically achieved after approximately 60 generations.

As shown in the flowchart in Fig. 7, the optimisation process of the beam-column elements was carried out according to the following steps:

- 1) The GA generates a population of cross-sectional shapes. In the initial step this population is assigned random characteristics (chromosomes), while subsequent generations are obtained as offspring of the previous one.
- 2) The gross cross-section properties, including the centroid (y_0, z_0), the shear centre (y_c, z_c), the second moments of area (I_y, I_z), the torsional and warping constants (I_w, I_t) and the radii of gyration (i_y, i_z, i_0) are determined for each cross-section.
- 3) The properties of the effective cross-section ($A_{eff}, W_{eff,y}, W_{eff,z}$) and the corresponding shifts of the centroidal axes relative to the original centroid (e_{Ny}, e_{Nz}) are calculated.

A_{eff} , e_{Ny} and e_{Nz} are calculated under pure compression, while $W_{eff,y}$ and $W_{eff,z}$ are calculated for major axis and minor axis bending, respectively.

- 4) The design resistances of the cross-section for uniform compression ($N_{c,Rd}$) and bending about the y-axis ($M_{cy,Rd}$) and z-axis ($M_{cz,Rd}$) are calculated, as explained in Section 2.
- 5) A small initial eccentric compressive load (N_{Ed}) is applied to the beam-column and the corresponding major axis bending moment ($M_{y,Ed} = N_{Ed}e_y$), as well as the additional bending moments $\Delta M_{y,Ed}$ and $\Delta M_{z,Ed}$ caused by the shifts of the centroidal axes, are calculated.
- 6) If the cross-section fails to pass the cross-sectional check (Eq. 3), then the current level of N_{Ed} is taken as the resistance of the element. Otherwise, the next steps 7-10, carrying out the member stability check, are performed.
- 7) The reduction factors for the different types of global buckling (i.e. flexural buckling about the y-axis (χ_{Fy}) and z-axis (χ_{Fz}), torsional (χ_T), flexural-torsional (χ_{FT}) and lateral-torsional (χ_{LT}) buckling) are calculated, as relevant. For the singly symmetric prototypes ①, ② and ③ flexural buckling about the minor axis, as well as flexural-torsional buckling about the major axis, are the relevant modes under compression, while for the doubly symmetric prototypes ④, ⑤ and ⑥ flexural buckling about either principal axis or torsional buckling may occur.
- 8) Based on Step 7 the design buckling resistances of the element for pure compression ($N_{b,Rd}$) and pure bending ($M_{b,Rd}$) are computed.
- 9) The interaction factors (k_{yy} , k_{yz} , k_{zy} , k_{zz}) for combined compression and bending are calculated using Annex A of EN1993-1-1.
- 10) The member resistance against combined compression and bending is verified using Eqs. (15) and (16). If both equations are satisfied, the axial compressive force (N_{Ed}) is increased by a small increment and the procedure is repeated from Step 6. This loop is iterated until the

maximum capacity of the beam-column element is obtained, i.e. either Eq. (3) in Step 6 or Eqs. (15-16) reach their limit.

11) After the capacities of all cross-sections of a generation are obtained and the fitness function is evaluated for each cross-section, the GA generates a next generation (Step 1).

5 Optimisation of CFS single section beam-column elements

Table 1 lists the cross-sectional dimensions and the corresponding ultimate load bearing capacities of the CFS beam-columns obtained from the optimisation process for different lengths ($L = 3000$ mm and $L = 5000$ mm), plate thicknesses ($t = 1.5$ mm and $t = 3$ mm) and load eccentricities (e_y). By increasing the eccentricity of the load from zero to an arbitrarily large number ($e_y = 10^5$ mm), the response of the beam-column elements gradually transitions from pure axial behaviour towards flexure-dominated behaviour. For the highest load eccentricity used in this study, the elements can be considered to be pure beam elements for all practical purposes. In Fig. 8 the capacities of the beam-column members with optimised cross-sections (N_{Ed}) are compared to that of the conventional standard cross-section ($N_{Ed,s}$) with the same weight, previously introduced in Fig. 6. To allow a visual comparison, Fig. 9 illustrates the optimised cross-sections of the beam-columns with different lengths, thicknesses and load eccentricities. Based on the presented results, the following conclusions can be drawn:

- In general, optimum cross-sectional shapes of CFS elements used as beams (i.e. $e_y = 10^5$ mm) tend to adopt deep webs, while reducing the flange width to the minimum specified value of 50 mm, as shown in Fig. 9. However, when axial compression becomes more dominant (i.e. when reducing e_y), the optimised shapes gradually display wider flanges and longer lips, while reducing the web height. This avoids any of the plate elements being excessively slender under more uniform compressive stresses and triggering local buckling.
- Previous optimisation research on the cross-sectional compressive capacity of lipped channels (Ma et al., 2015) has indicated a tendency for the optimum shape to exhibit a zero shift of the effective

centroid, meaning that the centroids of the gross cross-section and the effective cross-section coincide. This is due to the fact that this shift causes additional bending and that the minor axis bending capacity of lipped channels is typically fairly limited. The same phenomenon is here observed for the lipped channels (section ②) for $L = 3000$ mm and $e_y = 0$, both for $t = 1.5$ mm and $t = 3$ mm. However, for $L = 5000$ mm the influence of global buckling becomes dominant to the extent that it is more advantageous to increase the section properties for minor axis bending and warping than to maximize the cross-sectional capacity by minimizing the shift of the effective centroid. It is in this respect noted that flexural-torsional buckling is the governing buckling mode for all sections in Fig. 9 under compression.

- The adopted optimisation method led to the highest gains in capacity for pure axial compression (i.e. $e_y = 0$) using the optimised cross-sections ② and ③. Increases in ultimate capacity in the range of 40-60% were obtained compared to the conventional standard section. As expected, the beam-columns with optimised plain channel sections (①) are always less efficient than those with single- and double-fold edge stiffeners (② and ③).
- For the thinner sections ($t = 1.5$ mm) incorporating double-fold edge stiffeners (③) brings a modest but definite benefit over single-fold edge stiffeners (②), with a further increase in capacity of up to 12%. This is attributable to the susceptibility of the cross-section to distortional buckling, as well as to local buckling of the stiffener itself. However, for the thicker 3.0 mm sections the results indicate that, with the exception of pure compression, adding the extra fold in prototype ③ slightly reduces the capacity of the beam-columns compared to cross-sections with simple edge stiffeners (②), indicating that the extra material in the outstand lip can be more efficiently used elsewhere.
- The optimum angle θ of the lip in sections ② and ③ is invariably larger than 90° , resulting in outward-pointing lips. This configuration increases both the bending and warping properties of the

cross-section. However, it should be pointed out that previous studies (Ma et al., 2015) have demonstrated that the influence of this variable is rather limited.

6 Optimisation of CFS built-up and RHS beam-column elements

Table 2 lists the dimensions of the optimum CFS built-up members and optimum RHS members with various plate thicknesses and lengths, subject to various load eccentricities (e_y). To assess the gains in capacity resulting from the presented optimisation method, the capacities (N_{Ed}) of the beam-columns with optimised cross-sections are compared to the capacity ($N_{Ed,s}$) of the standard back-to-back channel section with the same material use (introduced in Fig. 6) in Table 2 and Fig. 10. The optimised shapes are also illustrated in Fig. 11.

Based on the results presented in Fig. 10 and Table 2, the following conclusions can be drawn:

- The back-to-back lipped channels exhibited trends similar to the single channels studied in Section 5. When increasing the applied bending moment on the beam-column relative to the amount of compression (i.e. when increasing the load eccentricity), the optimum cross-sections adopted deeper webs and, consequently, narrower flanges and lips. For the case of pure bending, all channels adopted the minimum specified flange width of 50 mm.
- In pure compression, the material is most efficiently used by the back-to-back lipped channels, which outperform the RHS. This is due to the slender walls of the RHS being quite susceptible to local buckling, both for $t = 1.5$ mm and $t = 3.0$ mm. The back-to-back channels maintain this advantage over most of the parameter ranges, but get slightly edged out by the RHS for $t = 3.0$ mm and intermediate eccentricities.
- The highest gains in capacity relative to the benchmark section were obtained with the back-to-back channels and the RHS for the longer spans ($L = 5000$ mm) under pure compressive loading (i.e. $e_y = 0$). Gains of up to 156% and 132% were achieved with the back-to-back channels and the RHS, respectively.

- By optimising the relative dimensions of the standard back-to-back channel section, the capacity of the beam-column was increased by up to 156% and 31% in pure compression ($e_y = 0$) and pure bending ($e_y = 10^5$ mm), respectively.
- The results show that the optimum angle θ of the lips of the back-to-back channel section (④) is always larger than 90° , resulting in outward-pointing lips.
- The optimum diamond-shaped cross-section (⑤) is, at best, capable of providing only a 7% increase in capacity compared to the standard section ($t = 1.5$ mm and $e_y = 0$). In almost all cases, the capacity of the optimum diamond-shaped section is lower than that of the benchmark section. This can mainly be attributed to its relatively low resistance to torsion, which in turn is due to the recognition that the presence of connectors at only discrete locations does not justify the torsional constant being calculated as if it were a closed section.
- In pure compression, the optimum RHS section is square. This is intuitively obvious, as flexural buckling about either cross-sectional axis is equally critical. Moreover, this configuration also maximizes the local buckling resistance, as moving towards a rectangular shape would increase the slenderness of two of the plates, thus promoting local buckling. In bending, on the other hand, the flanges take on the minimum specified width of 100 mm in an attempt to maximize the section depth.

7 Summary and conclusions

This paper explores the development of a practical optimization framework for the design of CFS beam-column members with different lengths and thicknesses, subject to various combinations of axial compression and bending moment. A GA optimisation method was used to obtain the best design solutions, while the European design guidelines (EC3) were used to evaluate the member capacity. Six different prototype cross-sections, including single channels, built-up channels and RHS were selected and individually optimised. Their relative dimensions and the inclination of the lip stiffeners were considered as the main design variables, while the EC3 dimensional limits and a range

of practical design requirements were taken into account as design constraints. The efficiency of the optimised beam-column cross-sections was benchmarked against a conventional commercially available channel with the same material use. Based on the presented results, the following conclusions can be made:

- The optimisation of CFS cross-sections to obtain increased capacity is a worthwhile endeavour, as gains in capacity of up to 156% were achieved. Even by simply changing the relative cross-sectional dimensions of the standard single and back-to-back lipped channel sections, the capacity of CFS beam-column elements was increased by up to 53%, and 156%, respectively, depending on the type of loading.
- As expected, lipped channels make more efficient use of the material than plain channels over the whole spectrum of lengths, thicknesses and load eccentricities. Adding an extra fold to create a return lip stiffener is beneficial for the more slender cross-sections ($t = 1.5$ mm) across the whole range of eccentricities, while for $t = 3.0$ mm the benefits are limited to the case of pure compression.
- It was observed in this study that under predominantly flexural loading optimum cross-sectional shapes tend to maximise the web height and use the minimum specified flange width. Conversely, in the transition towards pre-dominantly compressive loading the optimised shapes adopt stockier webs and wider flanges and lips. In this respect, it should be noted that deeper webs increase the susceptibility to web crippling and shear buckling. In the present study, members were subject to uniform bending. However, appropriate consideration needs to be made for these additional failure modes where specific situations demand it.
- The optimum cross-sectional shapes for $L = 3000$ mm and $L = 5000$ mm are not significantly different. From a commercial standpoint this is beneficial, as optimised cross-sectional shapes have the ability to deliver premium performance over a range of lengths.

- The optimised back-to-back channels could rival the performance of optimised RHS beam-columns with the same thickness over much of the range of eccentricities, the latter being hampered by local buckling of its walls. This was particularly true for the lower thickness ($t = 1.5$ mm).
- The optimised diamond-shaped cross-sections cannot compete with the back-to-back channel and RHS cross-sections in terms of efficiency over the studied parameter ranges. However, the simplified (and conservative) approach to calculating the torsion and warping properties of the diamond-shaped section in the present study should be noted.

Acknowledgment

This research was supported by the Engineering and Physical Sciences Research Council (EPSRC) grant EP/L019116/1. The first author was also supported by EPSRC Doctoral Scholarship grant 1625179. The authors thank the EPSRC for its financial support.

References

- Adeli, H. and Karim, A. (1997). "Neural network model for optimization of cold-formed steel beams". *J. Struct. Eng. ASCE* 123, 1535–1543.
- AISI S100-12 (2012). "North American specification for the design of cold-formed steel structural members". *American Iron and Steel Institute (AISI), Washington, DC, USA*.
- Andre, J., Siarry, P. and Dognon, T. (2001). "An improvement of the standard genetic algorithm fighting premature convergence in continuous optimization". *Advances in Engineering Software*, 32, 49-60.
- ANSI/AISC 360-10 (2010). "Specification for Structural Steel Buildings". *American Institute of Steel Construction (AISC)*.
- AS 4100:1990 Steel Structures (1990). "Standards Australia International Ltd". *New South Wales, Australia*.
- CEN (2005a). "Eurocode 3: design of steel structures, part 1.3: general rules—supplementary rules for cold formed members and sheeting, in, Brussels: European Committee for Standardization".
- CEN (2005b). "Eurocode 3: Design of Steel Structures. Part 1-1: General Rules and Rules for Buildings, in, Brussels: European Committee for Standardization".
- CEN (2006). "Eurocode 3: Design of steel structures, Part 1-5: Plated structural elements, in, Brussels: European Committee for Standardization".
- CEN (2020). "Eurocode 3: Design of Steel Structures. Part 1-1 (revision - final draft): General Rules and Rules for Buildings, in, Brussels: European Committee for Standardization".
- Cheng, S.-s., Kim, B. and Li, L.-y. (2013). "Lateral–torsional buckling of cold-formed channel sections subject to combined compression and bending". *Journal of Constructional Steel Research*, 80, 174-180.

- Gerald, F., T., A., Goodson, T. and Zsutty, M. (1989). "Slotted Bolted Connections in A seismic Design for Concentrically Braced Connections". *Earthquake Spectra*, 5, 383-391.
- Gilbert, B. P., Savoyat, T. J. M. and Teh, L. H. (2012a). "Self-shape optimisation application: Optimisation of cold-formed steel columns". *Thin-Walled Structures*, 60, 173-184.
- Gilbert, B. P., Teh, L. H. and Guan, H. (2012b). "Self-shape optimisation principles: Optimisation of section capacity for thin-walled profiles". *Thin-Walled Structures*, 60, 194-204.
- Goldberg, D. E. 1989. *Genetic algorithms in search, Optimization and machine learning*, Addison-Wesley.
- Holland, J. H. (1962). "Outline for a logical theory of adaptive systems". *Journal of ACM*, 9, 279-314.
- Karim, A. and Adeli, H. (1999). "Global optimum design of cold-formed steel hat-shape beams". *Thin-Walled Structures*, 35, 275-288.
- Lee, J., Kim, S.-M. and Seon Park, H. (2006). "Optimum design of cold-formed steel columns by using micro genetic algorithms". *Thin-Walled Structures*, 44, 952-960.
- Lee, J., Kim, S. M., Park, H. S. and Woo, B. H. (2005). "Optimum design of cold-formed steel channel beams using micro-genetic algorithm". *Eng. Struct*, 27, 17–24.
- Leng, J., Guest, J. K. and Schafer, B. W. (2011). "Shape optimization of cold-formed steel columns". *Thin-Walled Structures*, 49, 1492-1503.
- Leng, J., Li, Z., Guest, J. K. and Schafer, B. W. (2014). "Shape optimization of cold-formed steel columns with fabrication and geometric end-use constraints". *Thin-Walled Structures*, 85, 271-290.
- Li, Q.-Y. and Young, B. (2019). "Tests of cold-formed steel built-up open section beam-columns". *7th International Conference on Structural Engineering, Mechanics and Computation (SEMC 2019), September 2-4, 2019, Cape Town, South Africa*.
- Liu, H., Igusa, T. and Schafer, B. W. (2004). "Knowledge-based global optimization of cold-formed steel columns". *Thin-Walled Structures*, 42, 785-801.
- Ma, J.-L., Chan, T.-M. and Young, B. (2019). "Cold-Formed High-Strength Steel Rectangular and Square Hollow Sections under Combined Compression and Bending". *Journal of Structural Engineering*, 145, 04019154.
- Ma, W., Becque, J., Hajirasouliha, I. and Ye, J. (2015). "Cross-sectional optimization of cold-formed steel channels to Eurocode 3". *Engineering Structures*, 101, 641-651.
- Madeira, J. F. A., Dias, J. and Silvestre, N. (2015). "Multiobjective optimization of cold-formed steel columns". *Thin-Walled Structures*, 96, 29-38.
- Magnucki, K., Rodak, M. and Lewiński, J. (2006). "Optimization of mono- and anti-symmetrical I-sections of cold-formed thin-walled beams". *Thin-Walled Structures*, 44, 832-836.
- Mathworks 2011. Matlab R2011a. Mathworks, Inc.
- McKinstry, R., Lim, J. B. P., Tanyimboh, T. T., Phan, D. T. and Sha, W. (2015). "Optimal design of long-span steel portal frames using fabricated beams". *Journal of Constructional Steel Research*, 104, 104-114.
- McKinstry, R., Lim, J. B. P., Tanyimboh, T. T., Phan, D. T. and Sha, W. (2016). "Comparison of optimal designs of steel portal frames including topological asymmetry considering rolled, fabricated and tapered sections". *Engineering Structures*, 111, 505-524.

- Mojtabaei, S. M., Kabir, M. Z., Hajirasouliha, I. and Kargar, M. (2018). "Analytical and experimental study on the seismic performance of cold-formed steel frames". *Journal of Constructional Steel Research*, 143, 18-31.
- Mojtabaei, S. M., Ye, J. and Hajirasouliha, I. (2019). "Development of optimum cold-formed steel beams for serviceability and ultimate limit states using Big Bang-Big Crunch optimisation". *Engineering Structures*, 195, 172-181.
- Parastesh, H., Hajirasouliha, I., Taji, H. and Bagheri Sabbagh, A. (2019). "Shape optimization of cold-formed steel beam-columns with practical and manufacturing constraints". *Journal of Constructional Steel Research*, 155, 249-259.
- Pastor, M. M., Casafont, M., Chillarón, E., Lusa, A., Roure, F. and Somalo, M. R. (2009). "Optimization of cold-formed steel pallet racking cross-sections for flexural-torsional buckling with constraints on the geometry". *Engineering Structures*, 31, 2711-2722.
- Phan, D. K. (2020). "Strength and stiffness of built-up section columns. PhD thesis, The University of Sydney."
- Phan, D. T., Mojtabaei, S. M., Hajirasouliha, I., Ye, J. and Lim, J. B. P. (2019). "Coupled element and structural level optimisation framework for cold-formed steel frames". *Journal of Constructional Steel Research*, 105867.
- Sharafi, P., Teh, L. H. and Hadi, M. N. S. (2014). "Shape optimization of thin-walled steel sections using graph theory and ACO algorithm". *Journal of Constructional Steel Research*, 101, 331-341.
- Shir, O. M. 2012. Niching in Evolutionary Algorithms. In: ROZENBERG, G., BÄCK, T. & KOK, J. N. (eds.) *Handbook of Natural Computing*. Berlin, Heidelberg: Springer Berlin Heidelberg.
- Simões da Silva, L., Simoes, R. and Gervasio, H. (2010). "Design of Steel Structures, Eurocode 3: Design of Steel Structures, Part 1-1: General rules and rules for buildings, Ernst & Sohn - A Wiley Company". *ECCS Eurocode Design Manuals*.
- Tian, Y. S. and Lu, T. J. (2004). "Minimum weight of cold-formed steel sections under compression". *Thin-Walled Structures*, 42, 515-532.
- Torabian, S., Fratamico, D. C. and Schafer, B. W. (2016). "Experimental response of cold-formed steel Zee-section beam-columns". *Thin-Walled Structures*, 98, 496-517.
- Torabian, S., Zheng, B. and Schafer, B. W. (2015). "Experimental response of cold-formed steel lipped channel beam-columns". *Thin-Walled Structures*, 89, 152-168.
- Tran, T. and Li, L.-y. (2006). "Global optimization of cold-formed steel channel sections". *Thin-Walled Structures*, 44, 399-406.
- Wang, B., Bosco, G. L., Gilbert, B. P., Guan, H. and Teh, L. H. (2016a). "Unconstrained shape optimisation of singly-symmetric and open cold-formed steel beams and beam-columns". *Thin-Walled Structures*, 104, 54-61.
- Wang, B., Gilbert, B. P., Guan, H. and Teh, L. H. (2016b). "Shape optimisation of manufacturable and usable cold-formed steel singly-symmetric and open columns". *Thin-Walled Structures*, 109, 271-284.
- Wang, B., Gilbert, B. P., Molinier, A. M., Guan, H. and Teh, L. H. (2016c). "Shape optimisation of cold-formed steel columns with manufacturing constraints using the Hough transform". *Thin-Walled Structures*, 106, 75-92.
- Way, A. G. J. and Lawson, R. M. (2013). "Design and installation of light steel external wall systems". *SCI Guide ED-017*.

- Ye, J., Becque, J., Hajirasouliha, I., Mojtabaei, S. M. and Lim, J. B. P. (2018a). "Development of optimum cold-formed steel sections for maximum energy dissipation in uniaxial bending". *Engineering Structures*, 161, 55-67.
- Ye, J., Hajirasouliha, I., Becque, J. and Eslami, A. (2016a). "Optimum design of cold-formed steel beams using Particle Swarm Optimisation method". *Journal of Constructional Steel Research*, 122, 80-93.
- Ye, J., Hajirasouliha, I., Becque, J. and Pilakoutas, K. (2016b). "Development of more efficient cold-formed steel channel sections in bending". *Thin-Walled Structures*, 101, 1-13.
- Ye, J., Meza, F. J., Hajirasouliha, I., Becque, J., Shepherd, P. and Pilakoutas, K. (2019). "Experimental Investigation of Cross-Sectional Bending Capacity of Cold-Formed Steel Channels Subject to Local-Distortional Buckling Interaction". *Journal of Structural Engineering*, 145, 04019064.
- Ye, J., Mojtabaei, S. M. and Hajirasouliha, I. (2018b). "Local-flexural interactive buckling of standard and optimised cold-formed steel columns". *Journal of Constructional Steel Research*, 144, 106-118.
- Ye, J., Mojtabaei, S. M., Hajirasouliha, I., Shepherd, P. and Pilakoutas, K. (2018c). "Strength and deflection behaviour of cold-formed steel back-to-back channels". *Engineering Structures*, 177, 641-654.

List of Tables

Table 1. Optimisation results of single section beam-columns with different lengths, thicknesses and load eccentricities (all dimensions in mm)

L (mm)	t (mm)	e_y (10^3 mm)	optimum results*																
			Plain channel				Lipped channel					Channel with return lip							
			h	b	N_{Ed} (kN)	$\frac{N_{Ed}}{N_{Ed,s}}$	h	b	c	θ°	N_{Ed} (kN)	$\frac{N_{Ed}}{N_{Ed,s}}$	h	b	c	d	θ°	N_{Ed} (kN)	$\frac{N_{Ed}}{N_{Ed,s}}$
3000	1.5	0	246	103	33.11	0.64	193	81	49	111	75.18	1.46	161	82	49	15	91	81.54	1.58
		0.25	277	88	14.56	0.67	220	73	44	130	22.99	1.05	212	72	35	14	91	25.32	1.16
		1	299	77	6.00	0.68	259	67	29	117	9.02	1.02	239	64	31	12	90	10.01	1.13
		100	353	50	0.09	0.82	306	50	24	93	0.14	1.16	286	50	24	10	90	0.15	1.29
	3	0	246	104	100.90	0.84	132	100	60	106	180.84	1.51	158	82	49	16	93	185.98	1.55
		0.25	263	95	45.63	0.85	218	77	41	128	64.53	1.20	213	81	24	15	91	57.87	1.07
		1	284	85	19.22	0.83	244	72	32	126	24	1.04	233	74	22	14	90	23.17	1.00
		100	353	50	0.32	1.01	301	50	26	118	0.36	1.13	306	50	14	10	90	0.345	1.08
5000	1.5	0	236	108	22.07	0.80	198	80	48	118	41.96	1.53	136	89	53	17	91	42.42	1.54
		0.25	263	95	10.93	0.75	212	75	45	132	16.7	1.15	196	77	37	15	91	16.93	1.16
		1	275	89	4.99	0.70	240	67	40	133	7.42	1.04	216	74	31	14	90	7.79	1.09
		100	353	50	0.09	0.81	305	50	24	93	0.13	1.16	286	50	24	10	90	0.15	1.29
	3	0	236	108	60.13	0.97	154	93	56	110	86.38	1.40	169	79	48	15	92	90.29	1.46
		0.25	252	100	31.97	0.98	211	76	45	135	40.9	1.25	202	84	25	16	92	38.22	1.17
		1	257	98	15.37	0.89	227	72	41	135	19.35	1.12	213	81	23	15	91	18.12	1.05
		100	353	50	0.32	0.99	301	50	26	118	0.36	1.12	306	50	14	10	90	0.341	1.07

Table 2. Optimisation results of built-up and RHS beam-columns with various plate thicknesses, lengths and load eccentricities (all dimensions in mm)

L (mm)	t (mm)	e_y (10^3 mm)	optimum results *														
			Back-to-back channels						Diamond				RHS				
			h	b	c	θ°	N_{Ed} (kN)	$\frac{N_{Ed}}{N_{Ed,s}}$	h	b	θ°	N_{Ed} (kN)	$\frac{N_{Ed}}{N_{Ed,s}}$	h	b	N_{Ed} (kN)	$\frac{N_{Ed}}{N_{Ed,s}}$
3000	1.5	0	150	95	57	96	184.85	1.41	173	27	56	140.84	1.07	226	227	133.85	1.02
		0.25	243	66	39	116	50.81	1.11	176	25	60	38.64	0.85	312	141	48.19	1.05
		1	278	55	33	115	19.27	1.14	177	25	60	13.17	0.78	353	100	18.13	1.07
		100	306	50	24	92	0.27	1.31	177	25	60	0.15	0.73	353	100	0.22	1.06
	3	0	152	101	49	94	663.86	1.82	169	29	56	348.98	0.96	226	227	479.57	1.32
		0.25	208	86	37	116	146.35	1.14	177	25	60	102.93	0.80	312	141	157.82	1.23
		1	251	68	33	124	52.55	1.05	176	25	60	36.42	0.73	344	109	61.00	1.21
		100	304	50	24	110	0.72	1.12	177	25	60	0.43	0.67	353	100	0.71	1.11
5000	1.5	0	154	100	50	103	153.9	1.81	177	25	56	74.92	0.88	226	227	126.31	1.49
		0.25	208	77	46	123	41.05	1.20	177	25	60	28.78	0.84	309	144	41.53	1.22
		1	248	64	38	121	16.12	1.09	177	25	60	11.63	0.79	341	112	16.64	1.13
		100	306	50	24	94	0.27	1.29	177	25	60	0.15	0.73	353	100	0.22	1.06
	3	0	159	94	53	129	482.22	2.56	177	25	58	172.26	0.91	226	227	437.00	2.32
		0.25	190	89	43	128	119.23	1.40	177	25	59	72.73	0.85	277	176	139.84	1.64
		1	218	81	36	129	45.09	1.11	177	25	60	31.1	0.77	315	138	52.98	1.31
		100	304	50	24	115	0.71	1.12	176	25	60	0.43	0.67	353	100	0.71	1.11

List of Figures

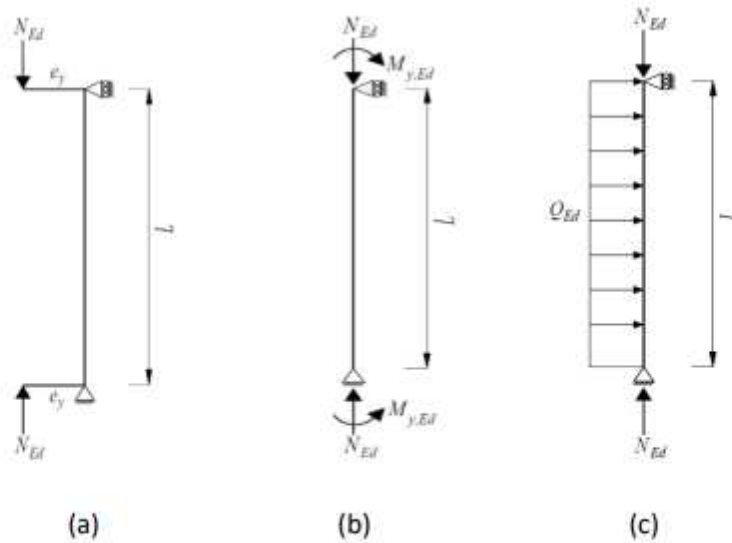


Fig. 1. Beam-column member subjected to; (a) axial compression with eccentricity; (b) combined axial compression and end moments; (c) combined axial compression and distributed transverse loads

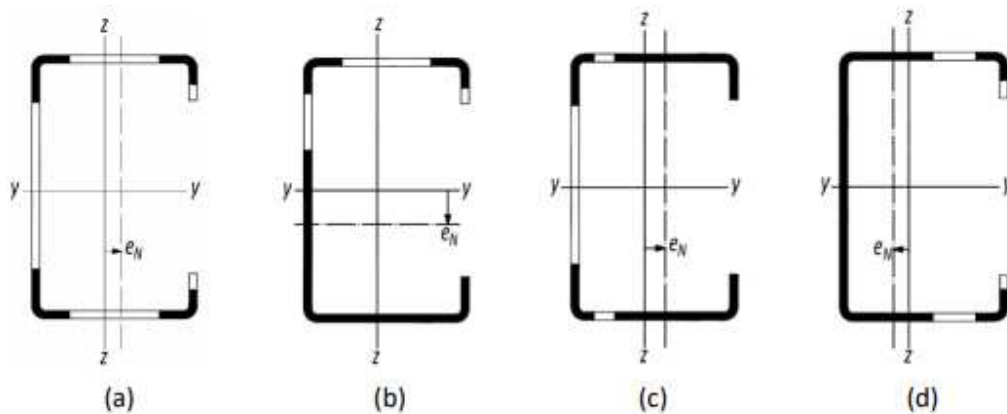


Fig. 2. Effective cross-section of a lipped channel subjected to: (a) axial compression; (b) bending about the major axis; (c) bending about the minor axis with the web in compression; and (d) bending about the minor axis with the web in tension

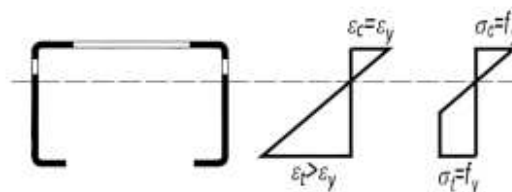


Fig. 3. Inelastic reserve capacity of a single CFS channel subjected to minor axis bending with the web in compression

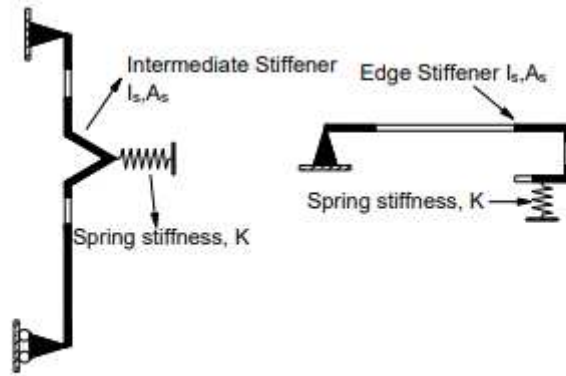


Fig. 4. Adopted EC3 model for distortional buckling calculations

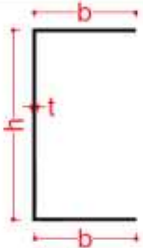
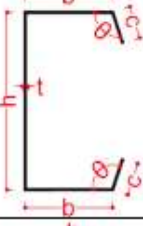
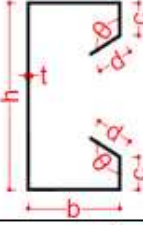
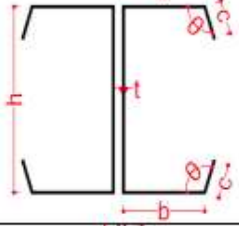
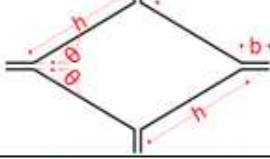
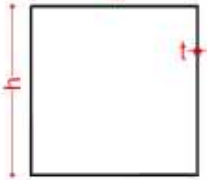
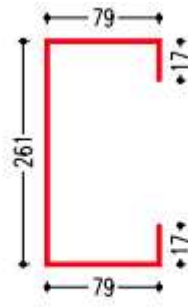
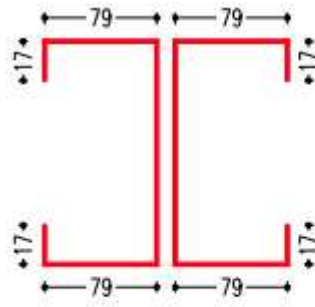
Cross-section No.	Cross-section shape	Total coil width (mm)	Design variables	Constraints based on EC3	Manufacturing & practical limitations (mm)	Buckling about axis	Buckling curve
①		453	$X_1 = b/L$	$b/t \leq 50$ $h/t \leq 500$	$b \geq 50$	Any	c
②		453	$X_1 = c/b$ $X_2 = b/L$ $X_3 = \theta$	$0.2 \leq c/b \leq 0.6$ $b/t \leq 60$ $c/t \leq 50$ $h/t \leq 500$ $\pi/4 \leq \theta \leq 3/4\pi$	$b \geq 50$ $c \geq 10$ $h \geq 2c \sin(\theta)$	Any	b
③		453	$X_1 = c/b$ $X_2 = d/b$ $X_3 = b/L$ $X_4 = \theta$	$0.2 \leq c/b \leq 0.6$ $0.1 \leq d/b \leq 0.3$ $b/t \leq 90$ $c/t \leq 60$ $d/t \leq 50$ $h/t \leq 500$ $\pi/4 \leq \theta \leq 3/4\pi$	$b \geq 50$ $c \geq 10$ $d \geq 10$ $h \geq 2c$	Any	b
④		906	$X_1 = c/b$ $X_2 = b/L$ $X_3 = \theta$	$0.2 \leq c/b \leq 0.6$ $b/t \leq 60$ $c/t \leq 50$ $h/t \leq 500$ $\pi/4 \leq \theta \leq 3/4\pi$	$b \geq 50$ $c \geq 10$ $h \geq 2c \sin(\theta)$	y z	a b
⑤		906	$X_1 = b/L$ $X_2 = \theta$	$b/t \leq 50$ $h/t \leq 500$	$b \geq 25$ $\pi/6 \leq \theta \leq \pi/3$	Any	b
⑥		906	$X_1 = b/L$	$b/t \leq 500$ $h/t \leq 500$	$b \geq 100$	Any	b

Fig. 5. Selected beam-column cross-sections, design variables, constraints and buckling curves



(a) Single channel



(b) Back-to-back channel

Fig. 6. Benchmark CFS beam-column cross-sections (dimensions in mm)

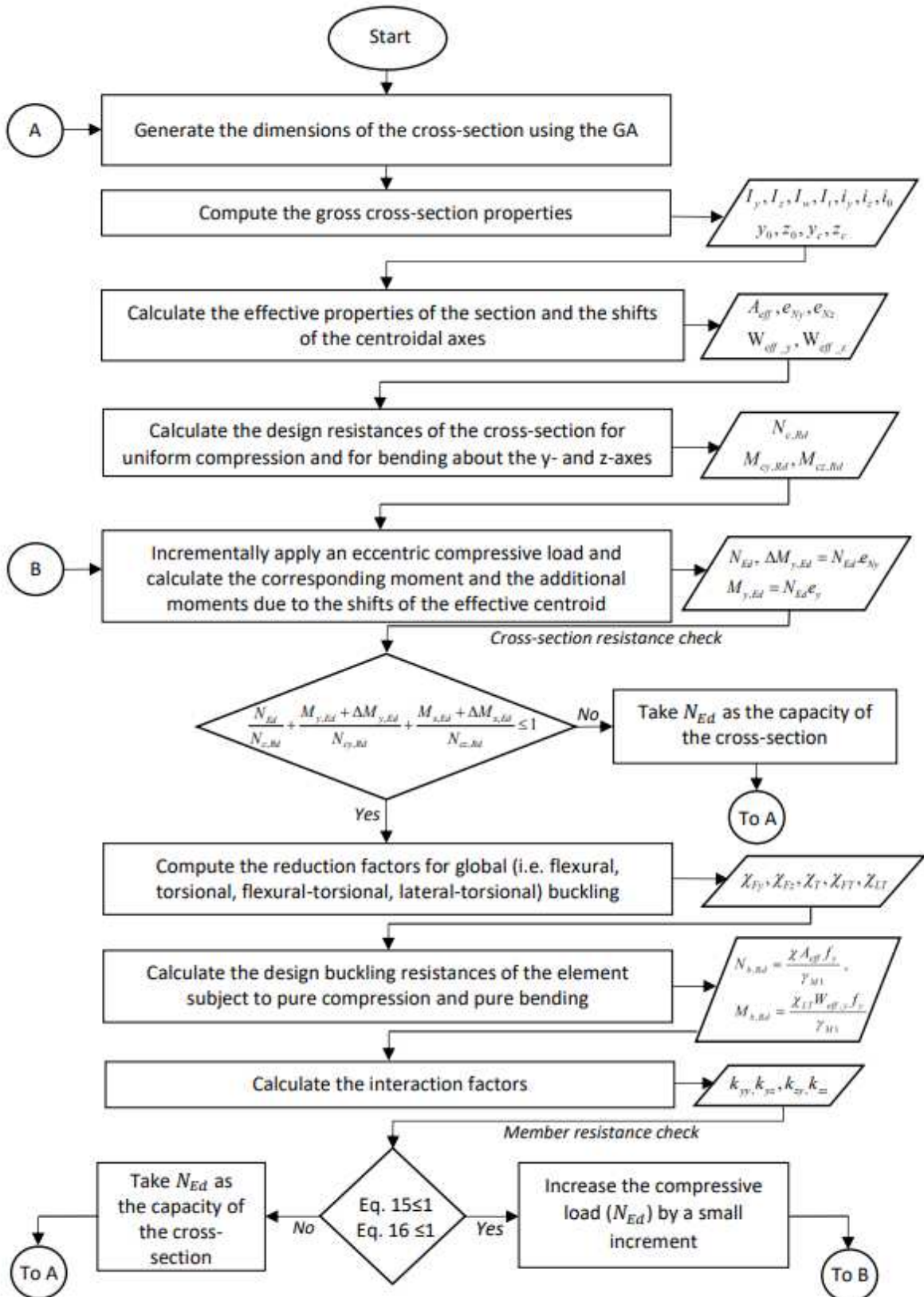


Fig. 7. Optimisation process flowchart for beam-column elements

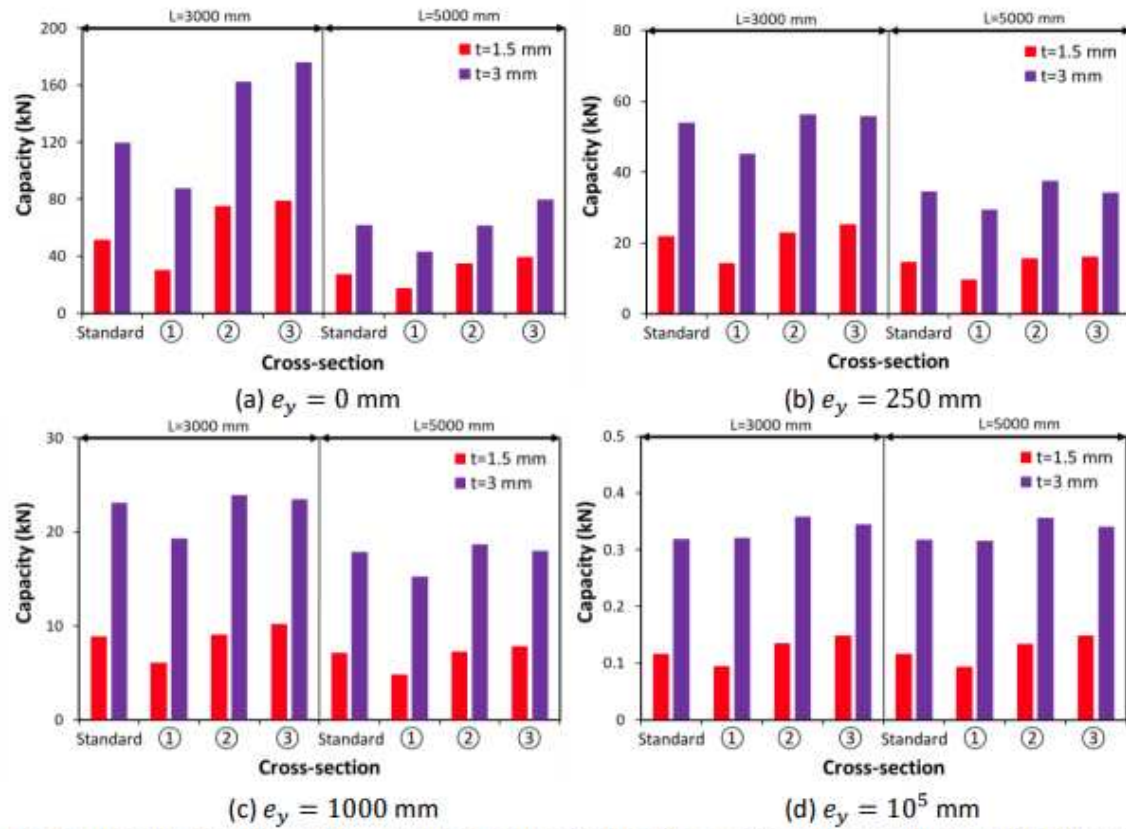


Fig. 8. Ultimate capacities of the standard and optimised single section beam-columns with different lengths, thicknesses and load eccentricities

Cross-section	t (mm)	$L = 3000$ (mm)				$L = 5000$ (mm)			
		$e_y = 0$ (mm)	$e_y = 0.25 \times 10^3$ (mm)	$e_y = 1 \times 10^3$ (mm)	$e_y = 100 \times 10^3$ (mm)	$e_y = 0$ (mm)	$e_y = 0.25 \times 10^3$ (mm)	$e_y = 1 \times 10^3$ (mm)	$e_y = 100 \times 10^3$ (mm)
①	1.5								
	3								
②	1.5								
	3								
③	1.5								
	3								

Fig. 9. Optimised shapes of single section beam-columns with different lengths, thicknesses and load eccentricities

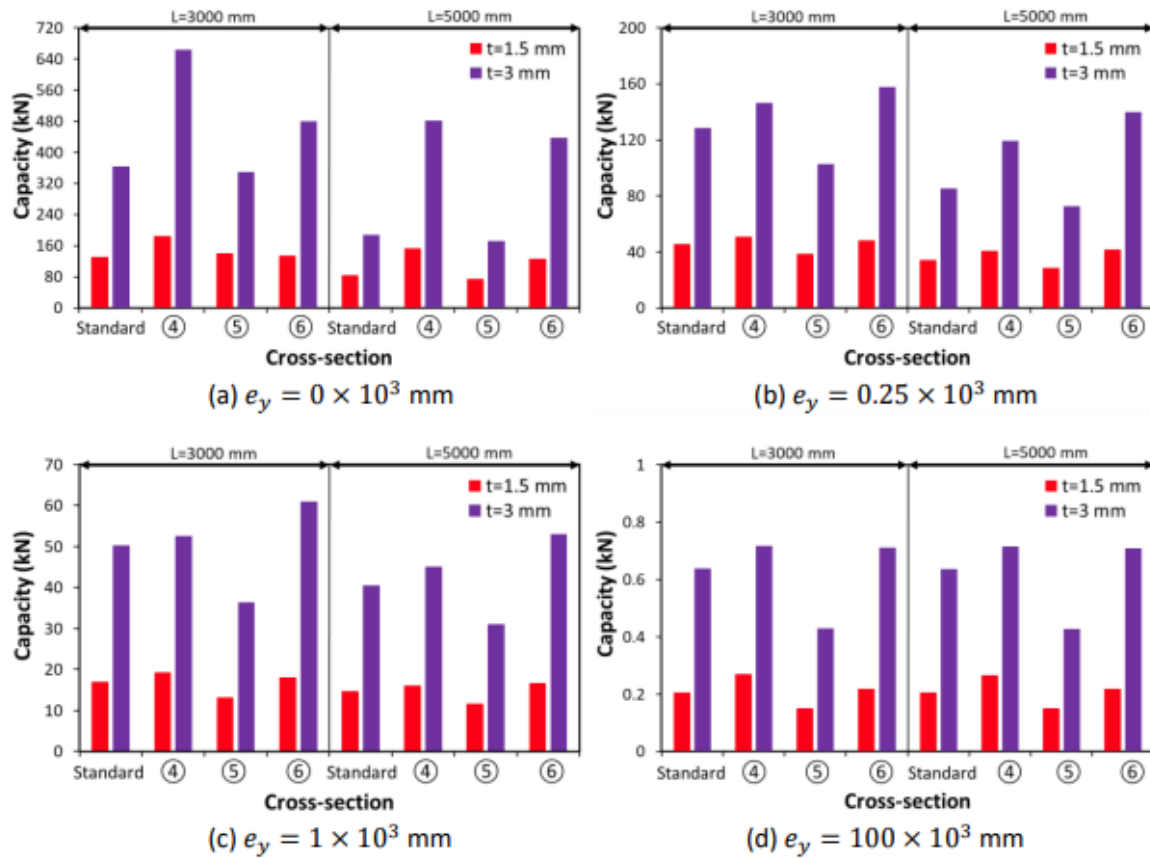


Fig. 10. Ultimate capacities of standard and optimised beam-columns with different lengths, thicknesses and load eccentricities

Cross-section	t (mm)	$L = 3000$ (mm)				$L = 5000$ (mm)			
		$e_y = 0$ (mm)	$e_y = 0.25 \times 10^3$ (mm)	$e_y = 1 \times 10^3$ (mm)	$e_y = 100 \times 10^3$ (mm)	$e_y = 0$ (mm)	$e_y = 0.25 \times 10^3$ (mm)	$e_y = 1 \times 10^3$ (mm)	$e_y = 100 \times 10^3$ (mm)
④	1.5								
	3								
⑤	1.5								
	3								
⑥	1.5								
	3								

Fig. 11. Optimised shapes of built-up and RHS beam-columns with different lengths, thicknesses and load eccentricities